Cellphone-Based Hand-Held Microplate Reader for Point-of-Care Testing of Enzyme-Linked Immunosorbent Assays

Brandon Berg,[†,‡] Bingen Cortazar,[†] Derek Tseng,[†,§] Haydar Ozkan,[†,§,∥] Steve Feng,[†] Qingshan Wei,[†,§] Raymond Yan-Lok Chan,[†] Jordi Burbano,[†] Qamar Farooqui,[†] Michael Lewinski,[§,⊥] Dino Di Carlo,[*,§,#,▽] Omai B. Garner,[*,⊗] and Aydogan Ozcan[*,†,§,#,○]

[†]Electrical Engineering Department, University of California, Los Angeles, California 90095, United States, [‡]Physics and Astronomy Department, University of California, Los Angeles, California 90095, United States, [§]Bioengineering Department, University of California, Los Angeles, California 90095, United States, [∥]Biomedical Engineering Department, Fatih Sultan Mehmet Vakif University, Istanbul 34445, Turkey, [⊥]Roche Molecular Systems, Inc., Pleasanton, California 94588, United States, [#]California NanoSystems Institute (CNSI), University of California, Los Angeles, California 90095, United States, [▽]Jonsson Comprehensive Cancer Center, University of California, Los Angeles, California 90095, United States, [⊗]Department of Pathology and Laboratory Medicine, David Geffen School of Medicine, University of California, Los Angeles, California 90095, United States, and [○]Department of Surgery, David Geffen School of Medicine, University of California, Los Angeles, California 90095, United States

ABSTRACT Standard microplate based enzyme-linked immunosorbent assays (ELISA) are widely utilized for various nanomedicine, molecular sensing, and disease screening applications, and this multiwell plate batched analysis dramatically reduces diagnosis costs per patient compared to nonbatched or nonstandard tests. However, their use in resource-limited and field-settings is inhibited by the necessity for relatively large and expensive readout instruments. To mitigate this problem, we created a hand-held and cost-effective cellphone-based colorimetric microplate reader, which uses a 3D-printed opto-mechanical attachment to hold and illuminate a 96-well plate using a light-emitting-diode (LED) array. This LED light is transmitted through each well, and is then collected *via* 96 individual optical fibers. Captured images of this fiber-bundle are transmitted to our servers through a custom-designed app for processing using a machine learning algorithm, yielding diagnostic results, which are delivered to the user within ∼1 min per 96-well plate, and are visualized using the same app. We successfully tested this mobile platform in a clinical microbiology laboratory using FDA-approved mumps IgG, measles IgG, and herpes simplex virus IgG (HSV-1 and HSV-2) ELISA tests using a total of 567 and 571 patient samples for training and blind testing, respectively, and achieved an accuracy of 99.6%, 98.6%, 99.4%, and 99.4% for mumps, measles, HSV-1, and HSV-2 tests, respectively. This cost-effective and hand-held platform could assist health-care professionals to perform high-throughput disease screening or tracking of vaccination campaigns at the point-of-care, even in resource-poor and field-settings. Also, its intrinsic wireless connectivity can serve epidemiological studies, generating spatiotemporal maps of disease prevalence and immunity.

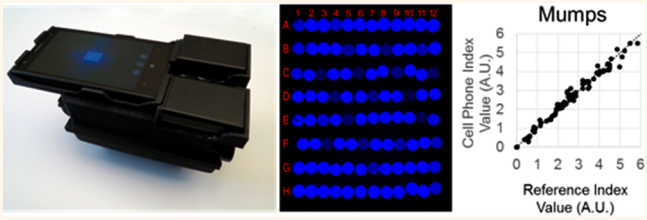

KEYWORDS: ELISA · immunoassay · point-of-care · microplate reader · smartphone · vaccination · telemedicine

Most of the commercially available technologies for point-of-care (POC) immunoassays center around lateral flow devices. Lateral flow immunoassays consist of prefabricated strips containing immobilized antigen and antibodies as well as nanoparticles.[1] The presence of an antibody in a specimen is recognized by binding to a region on the test strip and visualized using color-generating nanoparticle based labels. However, this simple testing method has some inherent weaknesses compared to enzyme-linked immunosorbent assay (ELISA) based tests. First, lateral flow assays (LFAs) are much less sensitive than ELISA because a larger amount of antibody–antigen interactions needs to occur to create a visible signal. Second, most of the commercially available LFAs provide qualitative analyte assessment. This limits the usefulness for vaccine effectiveness and many infectious disease diagnostics, because a semiquantitative or quantitative assessment is clinically important. Finally, LFA tests are only designed for single test use, which makes large-scale screening of

* Address correspondence to ozcan@ucla.edu, ogarner@mednet.ucla.edu, dicarlo@ucla.edu.

Received for review May 27, 2015 and accepted July 9, 2015.

Published online July 09, 2015
10.1021/acsnano.5b03203

populations based on LFA tests expensive and time-consuming.

Immunoserological analysis at the nanoscale is a critical component to diagnostic testing within a health care setting. Centralized laboratory testing by ELISA in a standard 96-well plate format allows for high-throughput and accurate antibody or antigen recognition for the diagnosis of many important infectious diseases, including herpes simplex virus (HSV), and vaccine effectiveness surveillance for re-emerging diseases such as measles and mumps.[2−4] These laboratories require a large, integrated infrastructure including robotic systems, liquid handlers, and multiwell scanning spectrophotometers to prepare and analyze samples in batch, which currently is only available in high resource capacity regions. POC immunoserological assays are available in resource limited settings, but these devices often sacrifice accuracy and can only test a limited number of patients. As the rate of infectious disease continues to increase in resource limited settings, there is a need for high-throughput and accurate POC antibody recognition and nanosensing platforms.

Various POC ELISA approaches have been developed recently based on *e.g.*, microfluidic platforms or paper-based devices, among others, in order to improve accessibility in resource-limited or remote areas.[5−10] Perhaps the most advanced work to date has also shown the ability to integrate a microfluidic ELISA platform with a smartphone dongle that could provide several functions including pumping and imaging of a silver precipitation readout of sandwich ELISA.[11] This approach was applied to triplex serological analysis achieving good agreement with gold standard ELISA testing. However, using a nonstandard disposable cartridge per patient remains relatively costly compared to standard multiwell plate based ELISA testing especially for community-wide screening and vaccine effectiveness monitoring efforts. The sensitivity of ELISA has also been tremendously improved in the past several decades with limits of detection approaching the single molecule limit by either compartmentalizing the assay into smaller volumes, a method known as the digital ELISA,[12,13] or by amplifying the color change, utilizing surface plasmon enhancement effect.[14]

Despite all the promising results obtained with these emerging approaches, 96-well plate based ELISA still remains the standard and most cost-effective tool in clinical laboratories for diagnosing diseases and monitoring the result of interventions, such as for vaccine efficacy screening. Even with an initially large capital investment, multiwell plate ELISAs are the standard format in clinical laboratories because sample batching and reduction in manual labor and consumables are extremely cost-effective. Additionally, multiwell plate implementations of a broad range of ELISA tests are already FDA-approved, easing future regulatory burden for adaptations of these tests.

Scanning based spectrophotometry is the standard method to read colorimetric ELISA signals from 96-well plates and it requires a relatively expensive and bulky benchtop reader to individually scan each well and a reliable power grid, seriously limiting the usefulness of this method in resource-limited or remote settings. Alternatively, imaging-based detection methods which capture the entire plate in a single shot by using either a digital camera[15−17] or a flatbed scanner[18] have been developed. Optical imaging methods are favorable for rapid diagnostic purposes; however, the miniaturization of these existing imaging systems into a self-contained and robust hand-held unit remains a major challenge due to the difficulty of creating a wide field of view (FOV) image that can span the entire plate area (127×85 mm^2) in a compact, lightweight and cost-effective design, with minimal optical aberrations. Moreover, the ideal POC well plate reader platform would also benefit from integrating additional functionalities such as on-site image processing, wireless connectivity, and a smart user-interface for immediate reporting, sharing, and spatiotemporal labeling/archiving, as well as visualization of diagnostic results for, *e.g.*, telemedicine and POC screening applications. Such a hand-held, cost-effective, and fully integrated plate reader system, however, has not yet been demonstrated.

Recent advances in consumer electronics and wireless communication devices have cultivated a transformation in biomedical imaging, sensing and diagnostics.[19] By leveraging the power of semiconductor sensor chips and carry-on optics, mobile-phone based devices have become a versatile microscopy/nanoscopy and sensing platform for a wide range of applications,[19−24] including blood analysis,[25,26] bacteria detection,[27] single-virus imaging,[28] DNA imaging and sizing,[29,30] chemical sensing,[31−34] and biomarker detection,[6,35,36] among others.[37−43] Smartphones have also been used to illuminate and image well-plate based ELISA tests.[44,45] However, these previous demonstrations are not hand-held and are in fact based on a bulky imaging geometry, which exhibits optical aberrations due to the large field-of-view, also degrading the sensitivity especially for wells that are closer to the edges of the multiwell plate. In general, it is also possible to use the camera of the mobile-phone to capture an image of the well-plate array in ambient light conditions or using an external lamp without an additional optical design.[46] However, this simple approach has severe limitations in terms of repeatability and detection sensitivity, both of which will depend on (i) the user (*e.g.*, in the form of uncontrolled variations in camera field-of-view and related tilts and motion artifacts), and (ii) the external lighting conditions (*e.g.*, day *vs* night). As a result of these limitations, no results from patient testing have been reported so far with this simple camera based standard multiwell plate imaging approach with ambient light.

Here, we demonstrate a cost-effective and hand-held smartphone-based colorimetric reader for rapid monitoring of microtiter plate (MTP) based colorimetric ELISA immunoassays. We created a unique optical fiber array based smartphone attachment to capture the transmitted light from each well of the MTP by the smartphone camera. When compared with other microplate readers, this design provides a significantly more compact and lightweight imaging platform, and does not suffer from optical aberrations since the 96-well plate is transformed into an imaging area at the end of the fiber-bundle that is >110-fold smaller compared to the actual area of the well plate. Our device utilizes blue LEDs as the light illumination array and is operated completely by battery power. We demonstrated the application of this device for monitoring four common clinical ELISA tests: measles IgG, mumps IgG, and herpes simplex virus IgG (*i.e.*, HSV1 and HSV2). We also created a Windows phone based smart app that can return the *quantitative* clinical index values calculated from a calibration curve and the qualitative Positive/Equivocal/Negative tripartite diagnostic decisions *via* a machine learning algorithm. By comparing the test results of our mobile-phone reader with the readout from a benchtop FDA approved clinical plate reader, we achieved an overall accuracy of 99.6%, 98.6%, 99.4%, and 99.4% for mumps, measles, HSV-1, and HSV-2 tests, respectively. This mobile device that is designed to read the colorimetric end point of a 96 well plate format could easily expand to other FDA-approved ELISA kits for disease diagnosis in POC testing, potentially revolutionizing high-throughput testing and nanosensing capabilities in low-resource and field-settings.

RESULTS AND DISCUSSION

Optical Imaging Hardware. Our ELISA colorimetric system (Figure 1) is composed of a Windows based smartphone (Lumia 1020, Nokia), paired with a portable 3D printed attachment to package together optical components, and a cloud connected data processing server in communication with a custom mobile application that serves as an interactive user interface. The hand-held nature of our ELISA colorimetric reader allows for use in the field, away from sophisticated machinery, but the data processing speed is partially limited by the computational hardware and the software available for use on the cell phone. To resolve this partial limitation while also maintaining portability, we used a server for data processing and a wireless network (*e.g.*, cellular data, Wi-Fi) for data transfer between the server and the mobile application (see Figure 2).

Figure 1A illustrates our 3D printed device which consists of three separate parts: the top part, which primarily functions as the holder for the cell phone, the bottom of the device, which houses the fiber optic array, and the middle chamber to load a 96 well plate,

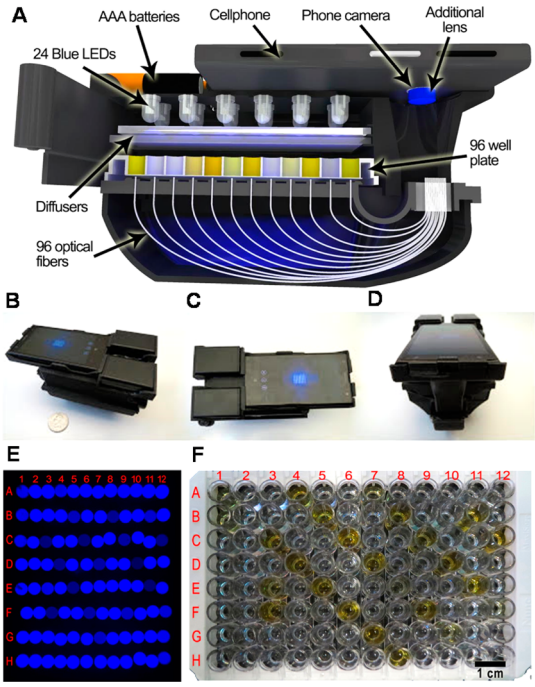

Figure 1. Schematic overview (A) and different perspectives (B–D) of the cellphone based ELISA colorimetric reader. Sample image (E), and sample plate (F). Rows and columns are labeled in (E) to correspond with the plate in (F).

which is illuminated vertically by an LED array consisting of 24 uniformly distributed blue LED's (peak wavelength, 464 nm). This system is powered using 6 AAA batteries and there is a low-noise, low-dropout linear current regulator in the system that provides constant power to all 24 LEDs. To maximize the uniformity of the illumination from the LED array, each LED is centered against 4 wells on the plate, and the illumination light was further homogenized by passing through two layers of plastic diffusers before reaching the plate. During each test, the 96-well ELISA plate of interest is inserted through the back of the device, as shown in Figure 1A. Blue light is transmitted through the well and is then coupled into the optical fibers, which guide the transmitted light to the external collection lens (focal length 45 mm) that is placed in front of the cellphone camera (upper right of Figure 1A). This fiber-optic imaging geometry yields a demagnification factor of approximately 11-fold within a rather compact and folded imaging design, which significantly reduces the height of the entire reader. The transmitted light through this fiber optic array is captured using the cellphone camera (41 megapixel, pixel size of 1.12 μm) in a RAW 10-bit/channel Digital Negative (DNG) image format. Figure 1E shows an example of an image taken by our system. The sample plate corresponding to this image is also shown in Figure 1F. The overall dimensions of our mobile reader are $\sim$195 $\times$ 98 $\times$ 100 mm^3. Figure 1B–D also shows different perspectives of the actual device with a US quarter used for scale comparison.

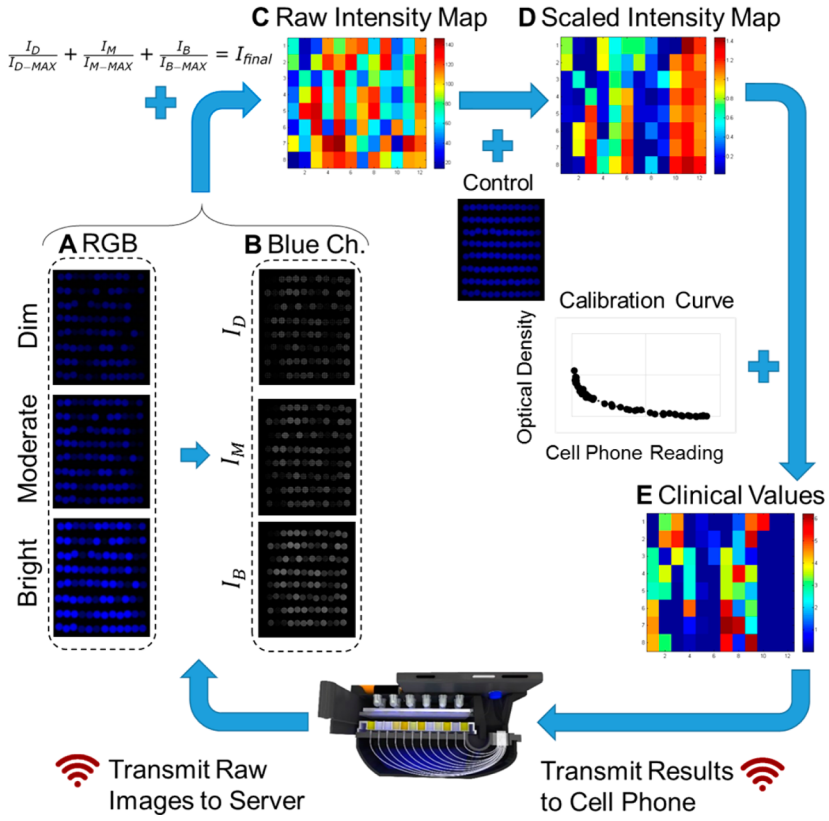

Figure 2. Flowchart showing the data processing steps of our reader. From the raw images (A), the blue channel (B) is extracted to be used for the rest of the data processing. Dividing the intensities of each well by the intensity of the brightest well, a raw intensity map (C) of blue pixel values is generated. Next, by normalizing everything to a control, a scaled intensity map of transmittances (D) is formed. Lastly, the transmittances are converted to clinical values (E) using a calibration curve.

A comparison of our cell-phone based ELISA reader against some of the commercially available ELISA readers[47−49] is also provided in the Supporting Information (Table S1). One of the smallest of these commercially available readers is the *Bio-Rad PR 4100*, which measures 134 × 347 × 187 mm^3 with a weight of 2.58 kg.[47] In comparison, our device design reduces the overall volume of the reader instrument by a factor of 4.54 and the weight by a factor of 4.17.

Data Processing *via* Smartphone Application and Server. Figure 2 illustrates the communication between the cellphone and the server, and the flowchart of data processing carried out in the server to obtain the final clinical quantitative values. First, the ELISA plate is inserted into the device and images are captured at three different exposure times (dim (τ_D) 1/1600 s, moderate (τ_M) 1/1250 s, and bright (τ_B) 1/800 s) using the Nokia Pro Camera application and saved on the phone using the RAW DNG image format (7152 × 5360 pixels) (Figure 2A). To process these images, the user runs our custom-developed application. Figure 3 shows screenshots of this colorimetric plate reader application: from the main menu (Figure 3A), the user can process a new test or review previously run tests. When starting a new test, the user first selects the dim, moderate, and bright images to use (see Figure 3B). Next, the user specifies the type of immunoassay being tested (*i.e.*, measles IgG, mumps IgG, HSV-1, or HSV-2 IgG), the column location of their tests in the well plate, and any conversion factors provided by the kit manufacturer, and then submits the test to the server for processing.

After receiving this new test request, the server (implemented in Python using the Twisted framework) waits for the DNG test files to finish uploading before processing. These DNG images are first converted to tagged image file format (TIFF) for easier extraction of the blue channel of the image. The blue channel pixel intensities (Figure 2B) are extracted from the raw images by localizing the Bayer pattern and defining its orientation. From the blue channel image, the average pixel intensity of each individual well is obtained. To do so, the centroids of each well are automatically detected using a custom designed algorithm. Since some centroids will randomly have low light intensity, a basic intensity thresholding method is not sufficient to accurately determine the position of all the 96 wells. Therefore, our custom-designed algorithm finds two reference centroids as ELISA plate markers using pixel intensity thresholding in combination with morphological erosion-dilation operations[50] to separate overlapping wells. We selected the most upper right and the most lower right wells as reference centroids, and using their coordinates, the algorithm is able to match the positions of all the remaining

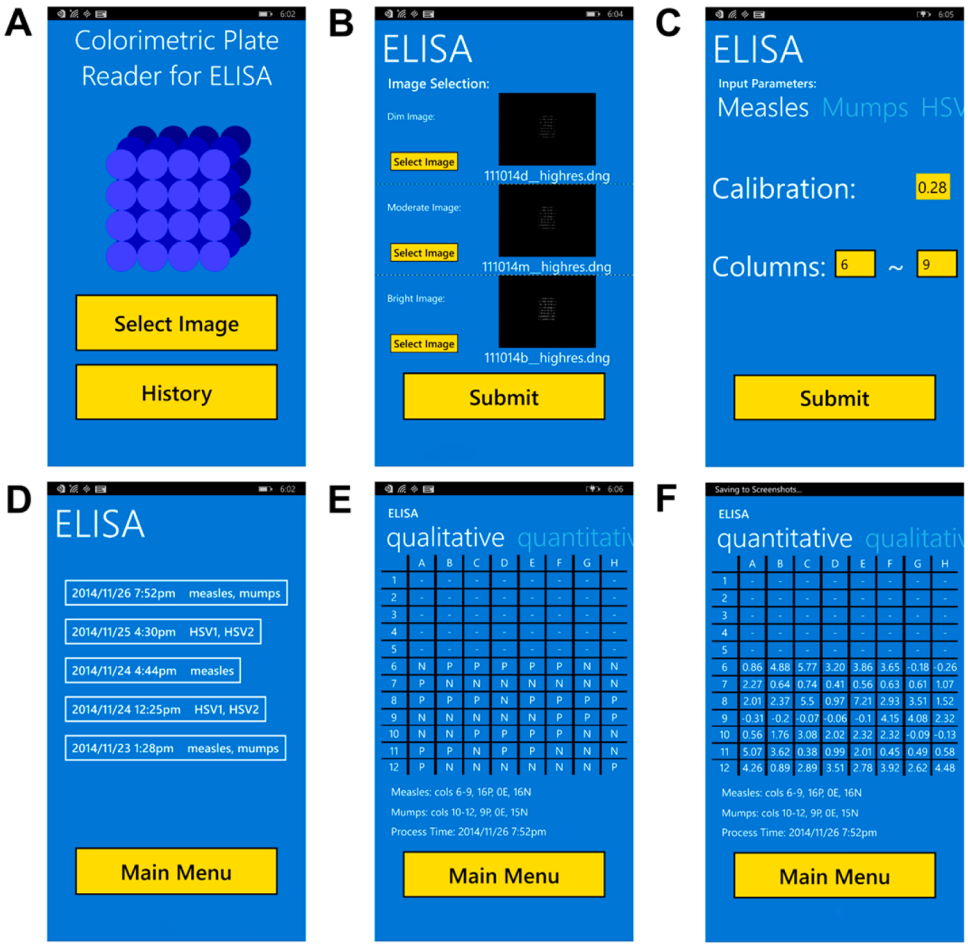

Figure 3. Screenshots from the Colorimetric Plate Reader app. (A) Main menu. (B) Image selection page for selecting the dim, moderate, and bright exposure images to start a new test. (C) Parameter page for selecting the assay type (*e.g.*, measles, mumps, HSV1, and HSV2), calibration values, and test column positions. (D) The history page displays submitted and processed tests on the server with their time of submission and test types. (E and F) Result display page showing either qualitative (*via* machine learning) or quantitative ELISA test results.

centroids by performing alignment/rotation corrections on 96 previously calculated blank plate centroids. Once these centroids are detected, a circular mask with a 15 pixel radius, which is a few pixels smaller than the radius of the well, is used to prevent edge related artifacts in our data processing.

Once the blue channel information is extracted, the dim, moderate, and bright average intensities per well (*i.e.*, I_D, I_M, and I_B, respectively) are combined to produce a high dynamic range (HDR) image. This is achieved through addition of each intensity after being scaled by the brightest well for that exposure time (Figure 2C), where $I_{D\text{-}MAX}$ is the highest well intensity of all the wells in the dim exposure time τ_D; $I_{M\text{-}MAX}$ and $I_{B\text{-}MAX}$ follow the same convention. To normalize against imaging system-induced changes on, *e.g.*, well transmittance, we also imaged blank reference wells with deionized (DI) water, which is a step performed only once for a given reader. After this normalization step, each cell in the scaled intensity map (Figure 2D) will have a value between 0 and 1. With the use of this scaling convention, a 1 represents complete transmittance relative to DI water control, while a 0 represents no transmittance reading.

The last step in our processing is to convert the optical density (OD) and transmittance values to a quantified index value used for clinical decisions. This conversion from OD to clinical index value is defined by the manufacturer of each immunoassay. The parameters used for this conversion to the final quantitative index value are the optical densities of three calibration wells and a test specific predetermined conversion factor. Finally, a matrix of these quantified clinical index values (one for each well) is transmitted back to the cell phone for the user to view through the same app (Figure 2E).

For the process of making qualitative clinical determinations, we have approached the problem using two different methods. The first method applies a threshold identical to the threshold of the original ELISA assay but based on the clinical index values obtained by our cellphone reader (Figure 2E). A clinical index value between 0.9 and 1.1 results in an equivocal determination, negative below 0.9, and positive

above 1.1. In addition to this curve-fitting and threshold based diagnostic decisions, we also employed a machine learning algorithm to make clinical determinations using a total of 58 spatial features that are automatically extracted from cellphone images. This second approach (Figure 4) makes no assumptions of a calibration function and increases its diagnostic accuracy as training sample size increases.

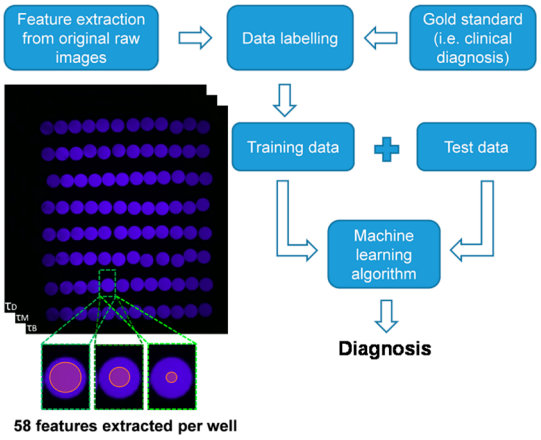

Figure 4. Flowchart of our machine learning decision algorithm.

The goal of this machine learning framework is to estimate the correct diagnostic label corresponding to each test set and every time a new test is performed, a test data set is created by extracting the same spatial features used for the training data set. We used an adaptive boosting machine learning algorithm,[51] which statistically learned from the training data set and estimated a diagnosis from each entry contained in the test data (see Figure 4). This algorithm provides accurate diagnosis by establishing statistical relations between the features of the training data set and the gold standard diagnostic labels. These statistical relationships are then applied to the features of the test data to make a blind diagnostic decision. The main advantage of using adaptive boosting based machine learning algorithms is their capability to detect the most promising features and discard others that may degrade the accuracy of the results. Consequently, the dimensionality of the statistical model is reduced and the accuracy of the final predictions is boosted.

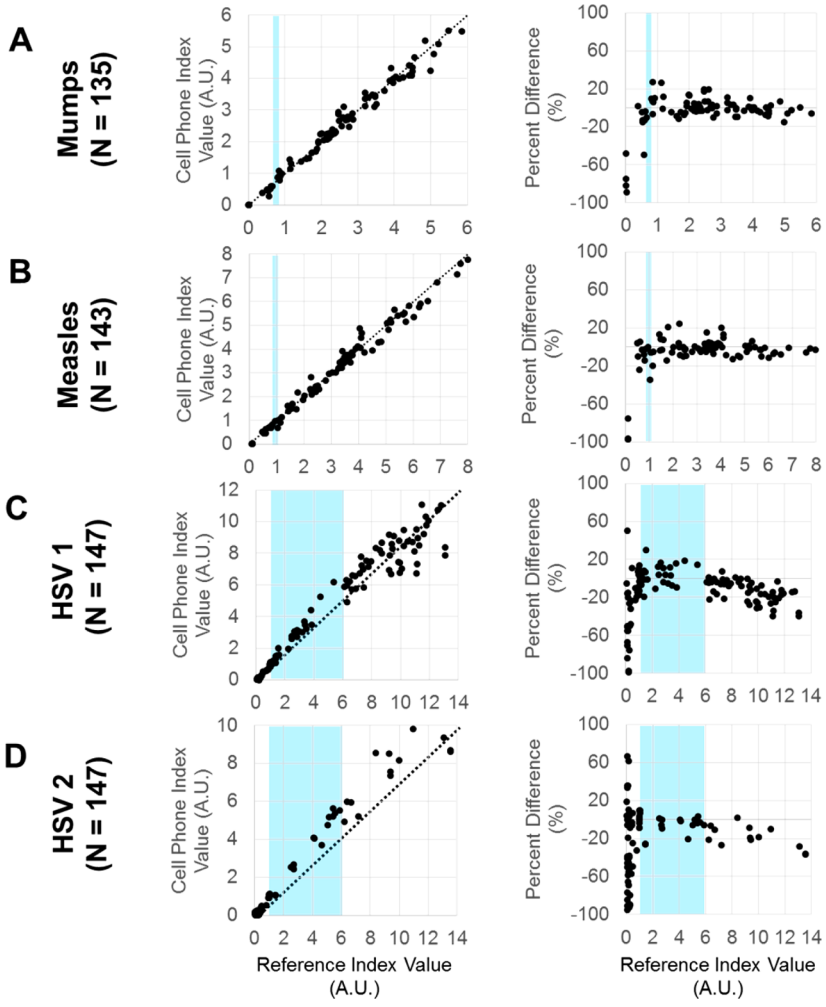

Figure 5. Comparison between the cell phone measured clinical values and the reference clinical values, measured by an FDA approved clinical spectrophotometer.

Clinical Testing. Our colorimetric cell-phone based system has shown the ability to reach high accuracy levels, ~99−100%, for the detection of measles IgG, mumps IgG, HSV-1 IgG, and HSV-2 IgG, with a total runtime of ~1 min on our server (Intel Core i5-760, 2.8 GHz, 16GB RAM) per each 96-well plate. Figure 5 shows our mobile-phone reader results obtained for these ELISA tests. The left column in Figure 5 represents the cell-phone index value *versus* the reference index value (both in arbitrary units), while the right column expresses the error detected between the results obtained by our mobile system and our gold standard, which is an FDA approved clinical spectrophotometer. On each graph, the clinically relevant linear-response region of each test, determined by their manufacturer, is also indicated.

Looking at the plots of the reference index value *versus* the cell phone measured index value shown in Figure 5, one can see that there is a strong correlation between the two readings and that there is an overlap, as expected, in the region of linearity between the two methods. The percentage difference plots shown in the right column of Figure 5 also illustrate that, as desired, there is no concentration dependent bias between the two measurement methods. Furthermore, outside of the blue highlighted ranges shown in Figure 5, a linear response is not expected for any read-out method or instrument, and that is why the deviation of the correlation between our mobile-phone based measurements and the reference method is not significant from the perspective of diagnostic classifications/decisions. In fact, as summarized in Table 1, by using thresholds in our clinical index value space, where $C < 0.9$, $C > 1.1$ and $0.9 < C < 1.1$ define negative, positive, and equivocal samples, respectively, we can achieve very strong agreements in our diagnostic decisions for all the tests against the gold standard well plate reader. These results can be further improved by analyzing the spatial features of the acquired cellphone images using a machine learning algorithm as detailed earlier. Indeed, Table 1 reports the significant improvements that we achieve in overall accuracy, specificity and sensitivity of our diagnostic decisions by replacing simple threshold based decisions with machine learning analysis, which take into account 58 spatial features for each test well to arrive a statistically trained and optimized ternary diagnostic decision.

According to Table 1, for mumps IgG samples, our machine learning algorithm achieves a 99.61% agreement to the FDA approved reference method. For measles samples, the agreement percentage is 98.56%. Similarly, for HSV-1 IgG and HSV-2 IgG results, we obtain agreements of 99.42% and 99.41%, respectively. The sensitivity and specificity performance of our machine learning approach is also better than the curve fitting based threshold approach, reaching >99% for HSV-1 IgG and HSV-2 IgG

TABLE 1. Qualitative Clinical Results[a]

	mumps		measles		HSV 1		HSV 2	
N	133		138		151		149	
analysis type	curve fitting	ML	curve fitting	ML	curve fitting	ML	curve fitting	ML
Specificity	92.70% ± 0.49%	97.37% ± 2.63%	92.09% ± 0.77%	94.56% ± 3.43%	100.00% ± 0.00%	100.00% ± 0.00%	100.00% ± 0.00%	100.00% ± 0.00%
Sensitivity	100.00% ± 0.00%	100.00% ± 0.00%	98.39% ± 0.42%	99.47% ± 0.59%	97.32% ± 0.32%	100.00% ± 0.00%	100.00% ± 0.00%	100.00% ± 0.00%
Agreement	97.21% ± 0.41%	99.61% ± 0.39%	96.08% ± 0.32%	98.56% ± 0.53%	97.16% ± 0.55%	99.42% ± 0.43%	98.66% ± 0.22%	99.41% ± 0.44%

[a] Percentages are shown with an error of one standard deviation. ML: Machine Learning.

tests. The relatively lower specificity of mumps IgG (97.37%) and measles IgG (94.56%) tests obtained from our machine learning approach can be partially attributed to the smaller sample sizes in these tests compared to HSV-1 IgG and HSV-2 IgG tests.

CONCLUSION

Using a cellphone and a 3D printed custom-designed opto-mechanical platform to illuminate and image a standard 96 well plate, we achieved an overall accuracy of ~99% or higher for HSV 1 IgG, and 99.4% for HSV 2 IgG tests. These results illustrate that our hand-held and cost-effective system is able to match the performance of a conventional FDA approved ELISA reader and give accurate diagnostic results to the users in approximately 1 min. Following the same calibration and testing procedures detailed in our Methods section, our system should be able to achieve similar results for other diseases normally tested *via* standard ELISA techniques.

These results are especially timely considering the recent re-emergence of measles. The United States has shown a 600% increase in measles cases in 2014 due to lack of regular vaccinations. It is critical from a public health perspective to know exactly how many people are effectively protected from measles to avoid further outbreaks. The presence of measles IgG (as assayed in this study) above an FDA defined threshold ensures protected status from this deadly reemerging disease. The availability of a hand-held and cost-effective multiwell plate reader allows for high-throughput vaccine surveillance outside of centralized areas and at the point of care. This is also critical in an outbreak to rapidly determine the number of susceptible (IgG negative) people immediately exposed to an active measles case. Measles is highly contagious in unvaccinated individuals and can have a mortality rate as high as 1:1000.

The mobile device reported in this study could also expand vaccination testing to rural areas that do not have access to centralized testing laboratories with large-scale spectrophotometers. The 96 well plate ELISA format is the gold standard for high-throughput antibody screening due to the extreme cost savings associated with batch testing and economies of scale compared to nonstandard or nonbatched cartridges or microchips. Our cellphone-based hand-held microplate reader brings this capability to resource limited areas and makes high-throughput point of care ELISA testing a reality. In addition, this device could be immediately useful in support of large-scale vaccination efforts in the developing world including trials and implementation of the tetravalent dengue vaccine. Such global health related efforts need to be coupled with a high-throughput, mobile and cost-effective ELISA screening device to ensure vaccine effectiveness and help eradicate disease.

One limitation of this work is that it relies on pipetting for loading of each well of the microplate of interest, and sample preparation and loading steps have not yet been integrated onto our mobile-phone based instrument. This limitation will be addressed in future work. Microfluidic automation can now perform complex liquid handling steps powered by simply drawing a vacuum in a syringe.[52] Furthermore, new methods for automated on-chip fluid manipulation such as acoustofluidic micromixing[53] and pumping[54] have been emerging, and commercial products have already integrated microfluidic systems into well plate formats.[55] Low-cost robotic liquid handler systems are also now becoming more commonplace, leveraging the consumer activities of the DIYBio and Maker communities[56] and the prevalence of low-cost microcontrollers (*e.g.*, Arduino).[57,58] Our current focus on the optical readout automation, replacing bulky and expensive multiwell scanning spectrophotometers with a hand-held design, addresses a key bottleneck in transitioning batched well-plate ELISA tests to field and resource poor settings, enabling standardization and economies of scale to act favorably outside of major urban centers in the U.S. and abroad.

METHODS

Study Design. We tested our colorimetric cell-phone based microplate reader platform in a clinical microbiology lab to demonstrate detection of measles IgG, mumps IgG, HSV-1 IgG, and HSV-2 IgG. Samples were prepared and tested at the UCLA Clinical Microbiology Laboratory using standard procedures for each test (Wampole Laboratories Mumps IgG ELISA II,[59] Wampole Laboratories Measles IgG ELISA II,[60] Focus Diagnostics HerpeSelect 1 ELISA IgG,[61] and Focus Diagnostics HerpeSelect 2 ELISA IgG[62]). For each disease, we quantified the performance of our approach by calculating accuracy, specificity and sensitivity values of our diagnostic decisions, where the results of an FDA approved well plate reader (DSX Automated ELISA system, Dynex Technologies) served as our gold standard. To minimize degradation of data quality due to elapsed time, all the clinical samples reported in this work were imaged by our mobile-phone platform in less than 30 min after the same sample was analyzed by the benchtop commercial plate reader. All these experiments were performed at UCLA Clinical Microbiology Laboratory by a medical personnel who did not develop the platform but was trained on how to operate our platform. For our performance calculations and comparisons, accuracy is defined as the number of true positives and true negatives divided by the total number of positives and negatives. Sensitivity is calculated as true positives divided by true positives plus false negatives, and specificity is calculated as true negatives divided by true negatives plus false positives. Note that since our gold standard technique sometimes is not able to accurately determine a positive or negative diagnosis, the equivocal test results of the reference technique are removed from our performance calculations, since these individual measurements do not present clinically interpretable results.

Calibration and Calculation of Test Results. For calibration of our platform, ELISA wells with known OD values were used. A comparison of Cell Phone Reading values (*C*) *versus* true OD

values obtained by our benchtop plate reader was established for each test to arrive at a calibration function. Calibration curves obtained for each IgG assay, which follow a logarithmic fitting that is based on the Beer's law, are presented in the Supporting Information (Figure S1). Each calibration curve maps the HDR normalized result obtained from our cell-phone system (*i.e.*, *C*) to the optical density value at 650 nm given by gold standard clinical reader. For each type of test, we used approximately half of the measurements for calibration and the other half for blind validation. On the top of each graph, the number of samples (*N*) used to build each calibration curve is also stated: 130 for mumps IgG, 133 for measles IgG, 154 for HSV-I IgG, and 150 for HSV-II IgG. Also note that the dynamic range for each IgG ELISA test is different: HSV-I IgG and HSV-II IgG cover a wide OD range between 0 and 4, while mumps and measles cover 0−3 and 0−2 ranges, respectively.

Machine Learning Algorithm. In our machine learning approach, a custom designed algorithm automatically detects each well center on the image, and calculates the average, standard deviation, maximum, minimum, and max−min difference of the blue channel intensities to be used as training features (Figure 4). In addition, as shown in Figure 2, each test consisted of three cellphone pictures at different exposure times (τ_D, τ_M, τ_B); so this feature extraction was repeated over these three images separately, including the resultant HDR value of each well used as additional features. Moreover, this process was repeated using three different circular mask dimensions (with 10, 15, and 25 pixel radius) over each well center (see Figure 4). Finally, the cell-phone clinical values (*C*) were also included in the feature pool, providing a total of 58 spatial features for characterization of each well.

Comparison of Diagnostic Decisions and Statistical Analysis. To compare the diagnostic performance of our mobile-phone based ELISA reader platform, we analyzed 10 random trials by splitting the available clinical measurement data in half for each disease. In other words, for each trial, half of the available data set was allocated toward training and the other half toward blind testing. This data splitting was carried out using a cross-validation technique[63] that provides optimized training sets. Due to the statistical nature of this cross-validation method, each trial has a different and randomly selected training set.

Finally, logarithmic calibration curve equations and *R*-Squared values reported in the Supporting Information were calculated using Microsoft Excel curve fitting tools.

Conflict of Interest: The authors declare the following competing financial interest(s): A.O. is the co-founder of a company that commercializes computational imaging and diagnostics technologies.

Acknowledgment. The authors acknowledge the NSF CBET Division Biophotonics Program, NSF Emerging Frontiers in Research and Innovation (EFRI) Award as well as the Howard Hughes Medical Institute (HHMI) Professors Program. This work is partially based upon research performed in a renovated laboratory by the National Science Foundation under Grant No. 0963183, funded under the American Recovery and Reinvestment Act of 2009. H. Ozkan also acknowledges TUBITAK scholarship.

Supporting Information Available: Calibration curves (Figure S1) converting measured cell phone transmittance into optical densities (one for each of the four diseases tested). Photographs of the device being tested at UCLA Clinical Microbiology Laboratory (Figures S2 and S3). Comparison of our cell-phone based ELISA reader against some of the commercially available readers (Table S1). The Supporting Information is available free of charge on the ACS Publications website at DOI: 10.1021/acsnano.5b03203.

REFERENCES AND NOTES

1. Ashley-Morrow, R.; Nollkamper, J.; Robinson, N. J.; Bishop, N.; Smith, J. Performance of Focus ELISA Tests for Herpes Simplex Virus Type 1 (HSV-1) and HSV-2 Antibodies among Women in Ten Diverse Geographical Locations. *Clin. Microbiol. Infect.* **2004**, *10*, 530–536.
2. Boteler, W. L.; Luipersbeck, P. M.; Fuccillo, D. A.; O'Beirne, A. J. Enzyme-Linked Immunosorbent Assay for Detection of Measles Antibody. *J. Clin. Microbiol.* **1983**, *17*, 814–818.
3. Ukkonen, P.; Väisänen, O.; Penttinen, K. Enzyme-Linked Immunosorbent Assay for Mumps and Parainfluenza Type 1 Immunoglobulin G and Immunoglobulin M Antibodies. *J. Clin. Microbiol.* **1980**, *11*, 319–323.
4. Posthuma-Trumpie, G. A.; Korf, J.; van Amerongen, A. Lateral Flow (Immuno)Assay: Its Strengths, Weaknesses, Opportunities and Threats. A Literature Survey. *Anal. Bioanal. Chem.* **2009**, *393*, 569–582.
5. Cheng, C.-M.; Martinez, A. W.; Gong, J.; Mace, C. R.; Phillips, S. T.; Carrilho, E.; Mirica, K. A.; Whitesides, G. M. Paper-Based ELISA. *Angew. Chem., Int. Ed.* **2010**, *49*, 4771–4774.
6. Gallegos, D.; Long, K. D.; Yu, H.; Clark, P. P.; Lin, Y.; George, S.; Nath, P.; Cunningham, B. T. Label-Free Biodetection Using a Smartphone. *Lab Chip* **2013**, *13*, 2124–2132.
7. Long, K. D.; Yu, H.; Cunningham, B. T. Smartphone Instrument for Portable Enzyme-Linked Immunosorbent Assays. *Biomed. Opt. Express* **2014**, *5*, 3792–3806.
8. Sun, S.; Yang, M.; Kostov, Y.; Rasooly, A. ELISA-LOC: Lab-on-a-Chip for Enzyme-Linked Immunodetection. *Lab Chip* **2010**, *10*, 2093–2100.
9. Wang, S.; Zhao, X.; Khimji, I.; Akbas, R.; Qiu, W.; Edwards, D.; Cramer, D. W.; Ye, B.; Demirci, U. Integration of Cell Phone Imaging with Microchip ELISA to Detect Ovarian Cancer HE4 Biomarker in Urine at the Point-of-Care. *Lab Chip* **2011**, *11*, 3411–3418.
10. Wang, T.; Zhang, M.; Dreher, D. D.; Zeng, Y. Ultrasensitive Microfluidic Solid-Phase ELISA Using an Actuatable Microwell-Patterned PDMS Chip. *Lab Chip* **2013**, *13*, 4190–4197.
11. Laksanasopin, T.; Guo, T. W.; Nayak, S.; Sridhara, A. A.; Xie, S.; Olowookere, O. O.; Cadinu, P.; Meng, F.; Chee, N. H.; Kim, J.; et al. A Smartphone Dongle for Diagnosis of Infectious Diseases at the Point of Care. *Sci. Transl. Med.* **2015**, *7*, 273re1.
12. Rissin, D. M.; Kan, C. W.; Campbell, T. G.; Howes, S. C.; Fournier, D. R.; Song, L.; Piech, T.; Patel, P. P.; Chang, L.; Rivnak, A. J.; et al. Single-Molecule Enzyme-Linked Immunosorbent Assay Detects Serum Proteins at Subfemtomolar Concentrations. *Nat. Biotechnol.* **2010**, *28*, 595–599.
13. Kim, S. H.; Iwai, S.; Araki, S.; Sakakihara, S.; Iino, R.; Noji, H. Large-Scale Femtoliter Droplet Array for Digital Counting of Single Biomolecules. *Lab Chip* **2012**, *12*, 4986–4991.
14. Chen, S.; Svedendahl, M.; Antosiewicz, T. J.; Käll, M. Plasmon-Enhanced Enzyme-Linked Immunosorbent Assay on Large Arrays of Individual Particles Made by Electron Beam Lithography. *ACS Nano* **2013**, *7*, 8824–8832.
15. Abriola, L.; Chin, M.; Fuerst, P.; Schweitzer, R.; Sills, M. A. Digital Imaging as a Detection Method for a Fluorescent Protease Assay in 96-Well and Miniaturized Assay Plate Formats. *J. Biomol. Screening* **1999**, *4*, 121–127.
16. Muttan, S.; Durai Arun, P.; Sankaran, K. Image Analysis System for 96-Well Plate Fluorescence Assays. *2012 Third International Conference on Computing Communication & Networking Technologies (ICCCNT)* **2012**, 1–6.
17. Durai Arun, P.; Sankaran, K.; Muttan, S. An Image Based Microtiter Plate Reader System for 96-Well Format Fluorescence Assays. *Euro. J. Biomed. Inf.* **2013**, *9*, en58.
18. Soldat, D. J.; Barak, P.; Lepore, B. J. Microscale Colorimetric Analysis Using a Desktop Scanner and Automated Digital Image Analysis. *J. Chem. Educ.* **2009**, *86*, 617.
19. Ozcan, A. Mobile Phones Democratize and Cultivate Next-Generation Imaging, Diagnostics and Measurement Tools. *Lab Chip* **2014**, *14*, 3187–3194.
20. Breslauer, D. N.; Maamari, R. N.; Switz, N. A.; Lam, W. A.; Fletcher, D. A. Mobile Phone Based Clinical Microscopy for Global Health Applications. *PLoS One* **2009**, *4*, e6320.
21. Smith, Z. J.; Chu, K.; Espenson, A. R.; Rahimzadeh, M.; Gryshuk, A.; Molinaro, M.; Dwyre, D. M.; Lane, S.; Matthews, D.; Wachsmann-Hogiu, S. Cell-Phone-Based Platform for Biomedical Device Development and Education Applications. *PLoS One* **2011**, *6*, e17150.

22. Vashist, S.; Mudanyali, O.; Schneider, E. M.; Zengerle, R.; Ozcan, A. Cellphone-Based Devices for Bioanalytical Sciences. *Anal. Bioanal. Chem.* **2014**, *406*, 3263–3277.
23. Preechaburana, P.; Suska, A.; Filippini, D. Biosensing with Cell Phones. *Trends Biotechnol.* **2014**, *32*, 351–355.
24. Erickson, D.; O'Dell, D.; Jiang, L.; Oncescu, V.; Gumus, A.; Lee, S.; Mancuso, M.; Mehta, S. Smartphone Technology Can be Transformative to the Deployment of Lab-on-Chip Diagnostics. *Lab Chip* **2014**, *14*, 3159–3164.
25. Zhu, H.; Mavandadi, S.; Coskun, A. F.; Yaglidere, O.; Ozcan, A. Optofluidic Fluorescent Imaging Cytometry on a Cell Phone. *Anal. Chem.* **2011**, *83*, 6641–6647.
26. Zhu, H.; Sencan, I.; Wong, J.; Dimitrov, S.; Tseng, D.; Nagashima, K.; Ozcan, A. Cost-Effective and Rapid Blood Analysis on a Cell-Phone. *Lab Chip* **2013**, *13*, 1282–1288.
27. Zhu, H.; Sikora, U.; Ozcan, A. Quantum Dot Enabled Detection of *Escherichia Coli* Using a Cell-Phone. *Analyst* **2012**, *137*, 2541–2544.
28. Wei, Q.; Qi, H.; Luo, W.; Tseng, D.; Ki, S. J.; Wan, Z.; Göröcs, Z.; Bentolila, L. A.; Wu, T.-T.; Sun, R.; et al. Fluorescent Imaging of Single Nanoparticles and Viruses on a Smart Phone. *ACS Nano* **2013**, *7*, 9147–9155.
29. Wei, Q.; Luo, W.; Chiang, S.; Kappel, T.; Mejia, C.; Tseng, D.; Chan, R. Y. L.; Yan, E.; Qi, H.; Shabbir, F.; et al. Imaging and Sizing of Single DNA Molecules on a Mobile Phone. *ACS Nano* **2014**, *8*, 12725–12733.
30. Selck, D. A.; Karymov, M. A.; Sun, B.; Ismagilov, R. F. Increased Robustness of Single-Molecule Counting with Microfluidics, Digital Isothermal Amplification, and a Mobile Phone *versus* Real-Time Kinetic Measurements. *Anal. Chem.* **2013**, *85*, 11129–11136.
31. Coskun, A. F.; Wong, J.; Khodadadi, D.; Nagi, R.; Tey, A.; Ozcan, A. A Personalized Food Allergen Testing Platform on a Cellphone. *Lab Chip* **2013**, *13*, 636–640.
32. Lee, S.; Oncescu, V.; Mancuso, M.; Mehta, S.; Erickson, D. A Smartphone Platform for the Quantification of Vitamin D Levels. *Lab Chip* **2014**, *14*, 1437–1442.
33. Wei, Q.; Nagi, R.; Sadeghi, K.; Feng, S.; Yan, E.; Ki, S. J.; Caire, R.; Tseng, D.; Ozcan, A. Detection and Spatial Mapping of Mercury Contamination in Water Samples Using a Smartphone. *ACS Nano* **2014**, *8*, 1121–1129.
34. Preechaburana, P.; Gonzalez, M. C.; Suska, A.; Filippini, D. Surface Plasmon Resonance Chemical Sensing on Cell Phones. *Angew. Chem., Int. Ed.* **2012**, *51*, 11585–11588.
35. Coskun, A. F.; Nagi, R.; Sadeghi, K.; Phillips, S.; Ozcan, A. Albumin Testing in Urine Using a Smart-Phone. *Lab Chip* **2013**, *13*, 4231–4238.
36. Oncescu, V.; O'Dell, D.; Erickson, D. Smartphone Based Health Accessory for Colorimetric Detection of Biomarkers in Sweat and Saliva. *Lab Chip* **2013**, *13*, 3232–3238.
37. Zhu, H.; Yaglidere, O.; Su, T.-W.; Tseng, D.; Ozcan, A. Cost-Effective and Compact Wide-Field Fluorescent Imaging on a Cell-Phone. *Lab Chip* **2011**, *11*, 315–322.
38. Mudanyali, O.; Dimitrov, S.; Sikora, U.; Padmanabhan, S.; Navruz, I.; Ozcan, A. Integrated Rapid-Diagnostic-Test Reader Platform on a Cellphone. *Lab Chip* **2012**, *12*, 2678–2686.
39. Shen, L.; Hagen, J. A.; Papautsky, I. Point-of-Care Colorimetric Detection with a Smartphone. *Lab Chip* **2012**, *12*, 4240–4243.
40. Rasooly, A.; Herold, K. E. *Mobile Health Technologies*; Springer: New York, 2015.
41. Park, T. S.; Li, W.; McCracken, K. E.; Yoon, J.-Y. Smartphone Quantifies *Salmonella* from Paper Microfluidics. *Lab Chip* **2013**, *13*, 4832–4840.
42. You, D. J.; Park, T. S.; Yoon, J.-Y. Cell-Phone-Based Measurement of TSH Using Mie Scatter Optimized Lateral Flow Assays. *Biosens. Bioelectron.* **2013**, *40*, 180–185.
43. Akl, T. J.; Wilson, M. A.; Ericson, M. N.; Farquhar, E.; Coté, G. L. Wireless Monitoring of Liver Hemodynamics *in Vivo*. *PLoS One* **2014**, *9*, e102396.
44. Vashist, S. K.; van Oordt, T.; Schneider, E. M.; Zengerle, R.; von Stetten, F.; Luong, J. H. T. A Smartphone-Based Colorimetric Reader for Bioanalytical Applications Using the Screen-Based Bottom Illumination Provided by Gadgets. *Biosens. Bioelectron.* **2015**, *67*, 248–255.
45. Su, K.; Zou, Q.; Zhou, J.; Zou, L.; Li, H.; Wang, T.; Hu, N.; Wang, P. High-Sensitive and High-Efficient Biochemical Analysis Method Using a Bionic Electronic Eye in Combination with a Smartphone-Based Colorimetric Reader System. *Sens. Actuators, B* **2015**, *216*, 134–140.
46. McGeough, C. M.; O'Driscoll, S. Camera Phone-Based Quantitative Analysis of C-Reactive Protein ELISA. *IEEE Trans. Biomed. Circ. Syst.* **2013**, *7*, 655–659.
47. PR 4100 Absorbance Microplate Reader. Bio-Rad. http://www.bio-rad.com/webroot/web/pdf/cdg/literature/R-782_PR-4100_Reader_Product_Sheet_DG12-0115.pdf (accessed June 23, 2015).
48. Dynamica Plate Reader - Halo LED 96. Dynamica. http://www.dynamica-eu.com/literatures/LEDetect_96_2008.pdf (accessed June 23, 2015).
49. Microplate Readers - Biochrom EZ Read LED Microplate Reader. Biochrom. http://www.biochrom.co.uk/product/101/biochrom-ez-read-led-microplate-reader.html (accessed June 23, 2015).
50. Haralick, R. M.; Sternberg, S. R.; Zhuang, X. Image Analysis Using Mathematical Morphology. *IEEE Trans. Pattern Anal. Mach. Intell.* **1987**, *9*, 532–550.
51. Mozos, O. M.; Stachniss, C.; Burgard, W. Supervised Learning of Places from Range Data Using Adaboost. *Proceedings of the 2005 IEEE International Conference on Robotics and Automation* **2005**, 1730–1735.
52. Duncan, P. N.; Nguyen, T. V.; Hui, E. E. Pneumatic Oscillator Circuits for Timing and Control of Integrated Microfluidics. *Proc. Natl. Acad. Sci. U. S. A.* **2013**, *110*, 18104–18109.
53. Huang, P.-H.; Xie, Y.; Ahmed, D.; Rufo, J.; Nama, N.; Chen, Y.; Chan, C. Y.; Huang, T. J. An Acoustofluidic Micromixer Based on Oscillating Sidewall Sharp-Edges. *Lab Chip* **2013**, *13*, 3847–3852.
54. Huang, P.-H.; Nama, N.; Mao, Z.; Li, P.; Rufo, J.; Chen, Y.; Xie, Y.; Wei, C.-H.; Wang, L.; Huang, T. J. A Reliable and Programmable Acoustofluidic Pump Powered by Oscillating Sharp-Edge Structures. *Lab Chip* **2014**, *14*, 4319–4323.
55. Spencer, C. I.; Li, N.; Chen, Q.; Johnson, J.; Nevill, T.; Kammonen, J.; Ionescu-Zanetti, C. Ion Channel Pharmacology under Flow: Automation *via* Well-Plate Microfluidics. *Assay Drug Dev. Technol.* **2012**, *10*, 313–324.
56. Lasercut and 3d Printed Parts. http://opensourcelaboratory.com/projects/pipettebot/instructions.html (accessed March 18, 2015).
57. Ito, S. A.; Carro, L. A Comparison of Microcontrollers Targeted to FPGA-Based Embedded Applications. *Proceedings of the 13th Annual Symposium on Integrated Circuits and Systems Design* **2000**, 397–402.
58. Molina-Markham, A.; Danezis, G.; Fu, K.; Shenoy, P.; Irwin, D. Designing Privacy-Preserving Smart Meters with Low-Cost Microcontrollers. In *Financial Cryptography and Data Security*; Springer: New York, 2012; pp 239−253.
59. Laboratory Procedure Manual: Mumps Antibody - Serum - Mumps IgG ELISA II. Center for Disease Control. http://www.cdc.gov/NCHS/data/nhanes/nhanes_09_10/MMRV_F_met_Mumps.pdf (accessed June 24, 2015).
60. Laboratory Procedure Manual: Measles Antibody - Serum - Measles IgG ELISA II. Center for Disease Control. http://www.cdc.gov/NCHS/data/nhanes/nhanes_09_10/MMRV_F_met_Measles.pdf (accessed June 24, 2015).
61. Herpeselect 1 ELISA IgG. Focus Diagnostics. https://www.focusdx.com/pdfs/pi/US/EL0910G.pdf (accessed June 24, 2015).
62. Herpeselect 2 ELISA IgG. Focus Diagnostics. https://www.focusdx.com/pdfs/pi/US/EL0920G.pdf (accessed June 24, 2015).
63. An, S.; Liu, W.; Venkatesh, S. Fast Cross-Validation Algorithms for Least Squares Support Vector Machine and Kernel Ridge Regression. *Pattern Recognit* **2007**, *40*, 2154–2162.